

Stochastic Model Predictive Control for Sub-Gaussian Noise

Yunke Ao ^{a,c,d}, Johannes Köhler ^b, Manish Prajapat ^{b,c,d}, Yarden As ^{c,d},
Melanie Zeilinger ^{b,d}, Philipp Fürnstahl ^{a,d}, Andreas Krause ^{c,d}

^a*ROCS, Balgrist University Hospital, University of Zurich, Switzerland*

^b*Institute for Dynamic Systems and Control, ETH Zurich, Zurich, Switzerland*

^c*Department of Computer Science, ETH Zurich, Zurich, Switzerland*

^d*ETH AI Center, ETH Zurich, Zurich, Switzerland*

Abstract

We propose a stochastic Model Predictive Control (MPC) framework that ensures closed-loop chance constraint satisfaction for linear systems with general *sub-Gaussian* process and measurement noise. By considering sub-Gaussian noise, we can provide guarantees for a large class of distributions, including time-varying distributions. Specifically, we first provide a new characterization of sub-Gaussian random vectors using *matrix variance proxies*, which can more accurately represent the predicted state distribution. We then derive tail bounds under linear propagation for the new characterization, enabling tractable computation of probabilistic reachable sets of linear systems. Lastly, we utilize these probabilistic reachable sets to formulate a stochastic MPC scheme that provides closed-loop guarantees for general sub-Gaussian noise. We further demonstrate our approach in simulations, including a challenging task of surgical planning from image observations.

Key words: Sub-Gaussian noise, Stochastic model predictive control, Probabilistic reachable sets, Optimal control synthesis for systems with uncertainty, Control of constrained systems, Output feedback control.

1 Introduction

Many real-world control systems operate in safety-critical environments. As such, these systems must maintain safety at all times, *even in light of stochasticity or model ambiguity*. Model Predictive Control (MPC) is a widely adopted optimization-based control framework, particularly well-suited for addressing challenges related to constraint satisfaction [29,28]. Robust and stochastic MPC techniques are commonly used to ensure constraint satisfaction in systems influenced by significant process and measurement noise.

Robust MPC approaches enforce satisfaction of safety guarantees under worst-case scenarios [23,16,30], often leading to overly conservative uncertainty propagation [5]. In contrast, stochastic MPC approaches model noise as random variables with stronger distributional assumptions and enforce constraints with a user-chosen probability, thereby reducing conservatism [13,24,12]. This work seeks to balance the need for reduced conservatism with weaker assumptions on the underlying noise distribution, by generalizing the existing stochastic MPC methods to sub-Gaussian noise.

Stochastic MPC has been widely studied [12,21,27,14], including theoretical results for closed-loop chance constraint satisfaction [13,24,15]. A common challenge in these frameworks is the computation of probabilistic reachable sets (PRS), i.e., sets containing future states with a high probability. Methods proposed by Hewing et al. and Muntwiler et al. leverage Gaussian distribution of the noise to derive PRS in closed-form [13,24]. However, the noise in real-world applications is often not Gaussian distributed. Lindemann et al. and Prandini et al. employ sampling-based techniques (confor-

* This work is in part supported by the Hasler Foundation ("Learn to learn safely" project, grant number: 21039), and Swiss National Science Foundation under NCCR Automation, grant agreement 51NF40 180545, and ETH AI Center.

Email addresses: yunke.ao@balgrist.ch (Yunke Ao), jkoehle@ethz.ch (Johannes Köhler), manishp@ai.ethz.ch (Manish Prajapat), yardas@ethz.ch (Yarden As), mzeilinger@ethz.ch (Melanie Zeilinger), Philipp.Fuernstahl@balgrist.ch (Philipp Fürnstahl), krausea@ethz.ch (Andreas Krause).

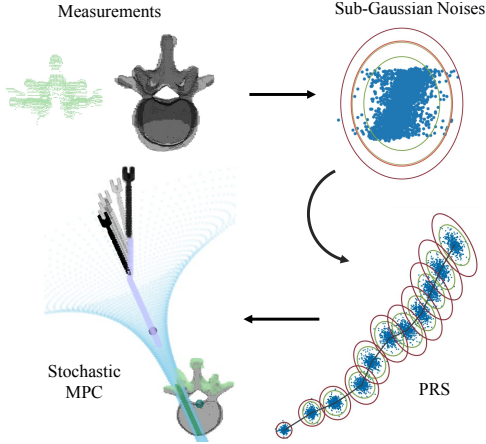


Fig. 1. Overview of the proposed stochastic MPC for sub-Gaussian noise at the example of the surgical planning (Section 4.1). We first obtain (high-dimensional) measurements and compute a sub-Gaussian characterization of the noise. Then, we provide a simple method to propagate uncertainty and compute probabilistic reachable sets (PRS, Section 3.2 and 3.3). The resulting probabilistic reachable sets of states are utilized in the stochastic MPC to provide probabilistic safety guarantees (Section 3.4).

mal prediction or scenario approach) under the assumption of independent and identically distributed (i.i.d.) noise [21,27]. Nevertheless, sampling-based methods can be computationally expensive for long-horizon problems and the i.i.d. assumption may be too restrictive in many applications. The Gaussian noise assumption can be relaxed using distributional robustness (DR) approaches, which can provide guarantees for families of distributions [22,3,17,18]. For instance, simple computations of PRS can be derived for general distributions using only the covariance, though the resulting sets tend to be conservative [17,13,11]. Aolaritei et al. recently incorporated samples and the Wasserstein distance to compute PRS, but the method still relies on i.i.d. noise assumptions [3].

Despite the advancements of existing works, limited work addresses closed-loop guarantees for MPC under *non-Gaussian* and *non-i.i.d.* noise. This challenge is particularly relevant for vision-based control, where states or intermediate observations are estimated from images and subsequently used to ensure safe control [8,19,10]. In such cases, estimation errors are in general non-Gaussian and non-i.i.d., as we further demonstrate later in Remark 1. To address this challenge, we draw on the concept of *light-tailed distributions*, widely used in machine learning and high-dimensional statistics [34,9], as a suitable characterization of such noise distributions. In particular, *sub-Gaussian* distributions encompass a broad class of light-tailed distributions (e.g., Gaussian) and all bounded distributions (e.g., the uniform distribution) [34]. Furthermore, note that sub-Gaussianity does not require that the noise is identically distributed.

In this work, we introduce a stochastic MPC framework for sub-Gaussian noise, see Figure 1 for an overview of the proposed approach. In particular, we extend the stochastic MPC framework [24] from Gaussian noise to handle general sub-Gaussian noise. We show that the resulting closed-loop system satisfies the chance constraints and provides a suitable bound on the asymptotic average performance. These results are enabled through our technical contributions:

- (i) New characterization of multivariate sub-Gaussian noise using *matrix* variance proxies;
- (ii) Linear propagation rules for the proposed matrix variance proxies;
- (iii) Probabilistic reachable sets and moment bounds for the proposed sub-Gaussian characterization.

Through numerical simulations, we demonstrate the advantages of our approach over existing stochastic, robust, and DR methods.

Notation: Let $\|x\|_V$ denote $\sqrt{x^\top V x}$ for $x \in \mathbb{R}^n$ and $V \in \mathbb{R}^{n \times n}$. Let $x_{0:t}$ be $x_0, x_1, x_2, \dots, x_t$. $\|V\|_2$ denotes the matrix norm of $V \in \mathbb{R}^{n \times n}$ induced by vector 2-norm. We use I to represent the identity matrix. Let $\lambda_{\max}(A)$ denote the maximum eigenvalue of the symmetric matrix A . We denote the expectation by \mathbb{E} . $\mathcal{N}(\mu, \Sigma)$ denotes the Gaussian distribution with mean μ and covariance matrix Σ . We use \mathbb{P}_x and $\mathbb{P}_{x|y}$ to denote the distribution of x and x given y respectively, i.e. $x \sim \mathbb{P}_x$ and $x \sim \mathbb{P}_{x|y}|y$. $\Pr\{E\}$ denotes the probability of an event E . Let \mathbb{N} denote the natural number set. We denote the Minkowski sum by \oplus . We use \mathcal{K}_∞ to denote the set of continuous functions $\alpha : \mathbb{R}_{\geq 0} \rightarrow \mathbb{R}_{\geq 0}$ which are strictly increasing, unbounded, and satisfy $\alpha(0) = 0$.

2 Problem statement

We consider the following linear time-invariant system:

$$x_{t+1} = Ax_t + Bu_t + w_t, \quad (1a)$$

$$y_t = Cx_t + \epsilon_t, \quad (1b)$$

where $t \in \mathbb{N}$ is the time step, $x_t \in \mathbb{R}^{n_x}$ is the state of the system, $y_t \in \mathbb{R}^{n_y}$ is the measurement, $u_t \in \mathbb{R}^{n_u}$ is the control input, $w_t \in \mathbb{R}^{n_x}$ are process noise and $\epsilon_t \in \mathbb{R}^{n_y}$ are measurement noise. The pair (A, B) is stabilizable and (A, C) is detectable. The states and inputs are subject to chance constraints:

$$\Pr\{x_t \in \mathcal{X}, u_t \in \mathcal{U}\} \geq 1 - \delta, \quad \forall t \in \mathbb{N}, \quad (2)$$

where \mathcal{X} and \mathcal{U} are safety-critical state and input constraint sets, $1 - \delta$ represents the user-specified satisfaction probability.

We consider sub-Gaussian noise distributions.

Definition 1 (σ -sub-Gaussian [34]). A real-valued random variable $X \in \mathbb{R}$ with mean μ and variance proxy σ is σ -sub-Gaussian, if, for all $s \in \mathbb{R}$, we have:

$$\mathbb{E}[\exp(s(X - \mu))] \leq \exp\left(\frac{\sigma^2 s^2}{2}\right). \quad (3)$$

A real-valued random vector $X \in \mathbb{R}^n$ is σ -sub-Gaussian, if the scalar $\lambda^\top X$ is σ -sub-Gaussian for all $\|\lambda\| = 1$.

We denote $\mathbb{P} \in \mathcal{SG}(\mu, \sigma)$ that a distribution \mathbb{P} is sub-Gaussian with mean μ and variance proxy σ . $\mathcal{SG}(\mu, \sigma)$ can characterize a whole class of distributions, such as Gaussian, uniform, and all bounded distributions. We assume that the initial state, measurement and process noise are (conditionally) sub-Gaussian with known variance proxies.

Assumption 1. For $x_0, w_{0:t}, \epsilon_{0:t}$ in system (1), we have:

$$\mathbb{P}_{x_0} \in \mathcal{SG}(\mu_0, \sigma_0), \quad (4a)$$

$$\mathbb{P}_{w_t | x_0, w_{0:t-1}, \epsilon_{0:t-1}, u_{0:t-1}} \in \mathcal{SG}(0, \sigma_w), \quad \forall t \in \mathbb{N}, \quad (4b)$$

$$\mathbb{P}_{\epsilon_t | x_0, w_{0:t-1}, \epsilon_{0:t-1}, u_{0:t-1}} \in \mathcal{SG}(0, \sigma_\epsilon), \quad \forall t \in \mathbb{N}, \quad (4c)$$

where $\mu_0 \in \mathbb{R}^{n_x}, \sigma_0, \sigma_w, \sigma_\epsilon > 0$ are known.

Note that Assumption 1 does not restrict the distributions of ϵ_t and w_t to be *identical over time*, as commonly assumed in stochastic MPC literature. Here σ_ϵ and σ_w are *common* sub-Gaussian variance proxies of measurement and process noises, respectively.

Overall, we consider the following stochastic optimal control problem:

$$\min_{\pi_0: \infty} \sum_{t=0}^{\infty} \ell(x_t, u_t) \quad (5a)$$

$$\text{s.t. } u_t = \pi_t(y_{0:t}, u_{0:t-1}), \quad (1), (2), (4), \quad \forall t \in \mathbb{N}, \quad (5b)$$

where ℓ is the stage cost and π_t are dynamic output-feedbacks. In this paper, we present a tractable approach to solving Problem 5.

Remark 1. The consideration of general sub-Gaussian noise (Assumption 1) allows for non-identical distributions, which are crucial to address nonlinear observations from images or point clouds, see also the example in Section 4.1. Specifically, suppose we have a non-linear observation $I_t = o(x_t) + \eta_t$ with i.i.d. noise η_t . Typically, we use a model-based algorithm or an offline learned inverse mapping, e.g. through neural networks [8], of the form

$$r(I_t) = r(o(x_t) + \eta_t) = Cx_t + \underbrace{r(o(x_t) + \eta_t) - Cx_t}_{=: \epsilon(x_t, \eta_t)}.$$

where the noise $\epsilon(x_t, \eta_t)$ depends on x_t . Then if $\epsilon(x_t, \eta_t)$ is bounded for all x_t and zero-mean, a common sub-Gaussian variance proxy σ_ϵ exists, such that $\mathbb{P}_{\epsilon(x_t, \eta_t) | x_t} \in \mathcal{SG}(0, \sigma_\epsilon)$ for all x_t , i.e., Assumption 1 holds. While the proposed approach can address such problems, this is not the case with state-of-the-art stochastic MPC approaches, which rely on identical noise distributions.

3 Method

In what follows, we develop our theory and analysis for solving Problem (5). We first provide a new definition of sub-Gaussian random variables using a *matrix variance proxy*. Further, in Section 3.2, we introduce linear propagation rules using such a matrix variance proxy. We then derive confidence bounds and moment bounds of the proposed new sub-Gaussian characterization in Section 3.3. These results are finally utilized to extend the state-of-the-art stochastic output-feedback MPC framework for Gaussian noise [24] to solve the Problem (5) (Section 3.4).

3.1 Sub-Gaussian with matrix variance proxy

Definition 1 characterizes sub-Gaussian random vectors with a scalar variance proxy σ . However, in linear systems (1), stochastic variances of states often develop correlations or scale differences across dimensions as they propagate through the dynamics. Consequently, relying on scalar variance proxies tends to overestimate uncertainty for state dimensions with smaller variance. To address this, we introduce a definition of sub-Gaussian random vectors using a matrix variance proxy.

Definition 2 (Sub-Gaussian with matrix (co-)variance proxy). A real-valued random vector $X \in \mathbb{R}^n$ with mean $\mathbb{E}[X] = \mu$ is called sub-Gaussian with a variance proxy $\Sigma \succeq 0$, i.e., $X \sim \mathcal{SG}(\mu, \Sigma)$, if $\forall \lambda \in \mathbb{R}^n$,

$$\mathbb{E}[\exp(\lambda^\top (X - \mu))] \leq \exp\left(\frac{\|\lambda\|_\Sigma^2}{2}\right). \quad (6)$$

Next, we show that Definition 2 generalizes the standard definition, i.e., Definition 1 is a special case of Definition 2.

Lemma 1. Every σ -sub-Gaussian random vector satisfying Definition 1 also has a finite matrix variance proxy $\Sigma = \sigma^2 I$ with Definition 2, and vice versa, i.e., every sub-Gaussian random vector having a matrix variance proxy $\Sigma \succ 0$ with Definition 2 is $\sqrt{\|\Sigma\|_2}$ -sub-Gaussian with Definition 1.

The proof of this lemma is detailed in Appendix A.1. Consequently, as *all distributions with bounded support* are sub-Gaussian noises under Definition 1 [34], they are also sub-Gaussian with a matrix variance proxy. We note that the multivariate sub-Gaussian stable distribution

[25,33] also uses positive definite matrices to characterize light-tailed distributions. However, this characterization can only capture elliptically contoured distributions [6], i.e., distributions whose probability mass contours are elliptically shaped, while Definition 2 has no such limitations. Moreover, contrary to Definition 2, this characterization does not contain the scalar sub-Gaussian definition as a special case.

3.2 Uncertainty propagation with linear systems

In System (1), states are propagated under linear transformation and addition. Here we show that sub-Gaussian distributions are closed under these operations and the resulting propagation of matrix variance proxy is also straightforward.

Theorem 1 (Propagation of matrix variance proxy). *Consider $X \sim \mathcal{SG}(\mu, \Sigma)$ (Definition 2) with $\mu \in \mathbb{R}^n$ and $\Sigma \succeq 0 \in \mathbb{R}^{n \times n}$.*

- a. For any matrix $A \in \mathbb{R}^{m \times n}$, $AX \sim \mathcal{SG}(A\mu, A\Sigma A^\top)$.
- b. If $\mathbb{P}_{Y|X} \in \mathcal{SG}(\mu', \Sigma')$, then $\mathbb{P}_{X+Y} \in \mathcal{SG}(\mu + \mu', \Sigma + \Sigma')$.

Proof. From Definition 2, we have for a:

$$\begin{aligned} \mathbb{E} [\exp(\lambda^\top A(X - \mu))] &\leq \exp\left(\frac{\|A^\top \lambda\|_\Sigma^2}{2}\right) \\ &= \exp\left(\frac{\|\lambda\|_{A\Sigma A^\top}^2}{2}\right). \end{aligned}$$

For b, it can be shown by:

$$\begin{aligned} &\mathbb{E} \left[\exp \left[\lambda^\top ((X - \mu) + (Y - \mu')) - \frac{\|\lambda\|_\Sigma^2}{2} - \frac{\|\lambda\|_{\Sigma'}^2}{2} \right] \right] \\ &= \mathbb{E}_X \left[\exp \left(\lambda^\top (X - \mu) - \frac{\|\lambda\|_\Sigma^2}{2} \right) \right] \\ &\quad \mathbb{E}_{Y|X} \left[\exp \left(\lambda^\top (Y - \mu') - \frac{\|\lambda\|_{\Sigma'}^2}{2} \right) \right] \\ &\stackrel{\text{Equ. (6)}}{\leq} \mathbb{E}_X \left[\exp \left(\lambda^\top (X - \mu) - \frac{\|\lambda\|_\Sigma^2}{2} \right) \cdot 1 \right] \stackrel{\text{Equ. (6)}}{\leq} 1. \quad \square \end{aligned}$$

Theorem 1 indicates that the propagation rule of matrix variance proxy is similar to the propagation of covariance matrices, enabling simple uncertainty propagation with linear systems. Propagation of sub-Gaussian noise under linear dynamics has also been studied for system identification [31], however, using a scalar variance proxy and without derivations of probabilistic reachable sets.

3.3 Confidence and moment bounds

In stochastic MPC, one key step for guaranteeing safety is computing probabilistic reachable sets (PRS), i.e., es-

tablishing confidence bounds \mathcal{E}_t^x for the state distributions with $\Pr\{x_t \in \mathcal{E}_t^x\} \geq 1 - \delta$. With Theorem 1, we can predict matrix variance proxies of state distributions in system (1). To compute PRS, we additionally need to derive confidence bounds using these obtained matrix variance proxies. Next, we present two confidence bounds for sub-Gaussian distributions.

Lemma 2 (Half-space bound). *If $X \sim \mathcal{SG}(\mu, \Sigma)$, then for any $h \in \mathbb{R}^n$, $\Pr\{X \in \mathcal{E}^h\} \geq 1 - \delta$ with the half-space confidence bound:*

$$\mathcal{E}^h(\mu, \Sigma, \delta, h) := \left\{ X \mid h^\top (X - \mu) \leq \|h\|_\Sigma \sqrt{2 \ln \frac{1}{\delta}} \right\}.$$

Proof. By Chernoff inequality, for any $s > 0$ and $\tau > 0$,

$$\begin{aligned} \Pr\{h^\top (X - \mu) \geq \tau\} &= \Pr\{\exp(sh^\top (X - \mu)) \geq \exp(s\tau)\} \\ &\leq \mathbb{E} [\exp(sh^\top (X - \mu) - s\tau)] \stackrel{\text{Equ. (6)}}{\leq} \exp\left(\frac{s^2 \|h\|_\Sigma^2}{2} - s\tau\right). \end{aligned}$$

Assigning $s = \frac{\tau}{\|h\|_\Sigma^2}$ gives:

$$\Pr\{h^\top (X - \mu) \geq \tau\} \leq \exp\left(-\frac{\tau^2}{2\|h\|_\Sigma^2}\right).$$

Then solving τ from $\exp\left(-\frac{\tau^2}{2\|h\|_\Sigma^2}\right) = \delta$ yields the confidence bound for $1 - \delta$. \square

Note that this bound recovers the known confidence bound for scalar variance proxy [34] as a special case.

Given Lemma 2, we could also construct polytope confidence sets as an intersection of individual half-space constraints using Boole's inequality [26]. To leverage the correlation between different dimensions, we also introduce elliptical confidence bounds using the variance proxy Σ more directly:

Theorem 2 (Elliptical bound). *Consider $X \sim \mathcal{SG}(\mu, \Sigma)$ with $\mu \in \mathbb{R}^n$ and $\Sigma \succ 0 \in \mathbb{R}^{n \times n}$, then we have for all $\tau > \sqrt{n}$:*

$$\Pr\{\|X - \mu\|_{\Sigma^{-1}} \geq \tau\} \leq \left(\frac{e}{n}\right)^{\frac{n}{2}} \tau^n \exp\left(-\frac{\tau^2}{2}\right) \quad (7)$$

Moreover, $\Pr\{X \in \mathcal{E}^e\} \geq 1 - \delta$ with the elliptical confidence bound:

$$\mathcal{E}^e(\mu, \Sigma, \delta, n) := \left\{ X \mid \|X - \mu\|_{\Sigma^{-1}}^2 \leq n + ng^{-1}(\delta^{-\frac{2}{n}}) \right\}, \quad (8)$$

where $g \in \mathcal{K}_\infty$, $g(x) = \frac{\exp x}{1+x}$.

The proof of this theorem is detailed in Appendix A.2. Moreover, Theorem 2 can also give a cylindrical set with bounds only in a subspace as

$$\mathcal{E}^e = \underbrace{H^\dagger \mathcal{E}^e(H\mu, H\Sigma H^\top, \delta, n_c)}_{=: \mathcal{E}^e(H, \mu, \Sigma, \delta, n_c)} \oplus \text{Null}(H), \quad (9)$$

where $H \in \mathbb{R}^{n_c \times n}$, $n_c < n$, H^\dagger denotes the pseudo-inverse of H , and $\text{Null}(H)$ represents the null space $\{x \in \mathbb{R}^n | Hx = 0\}$. Clearly, this set only has an elliptical boundary in the subspace $\text{span}(H)$ and unrestricted in $\text{Null}(H)$.

Similar to the Gaussian case, our sub-Gaussian confidence bound grows logarithmically w.r.t. δ^{-1} :

Corollary 1. *For all $\delta \in (0, 1)$, $n \geq 1$, the set \mathcal{E}^e in Theorem 2 satisfies*

$$\mathcal{E}^e(\mu, \Sigma, \delta, n) \subseteq \{X | \|X - \mu\|_{\Sigma^{-1}}^2 \leq (1 + \ln 4)n + 4 \ln \delta^{-1}\}.$$

The proof of this corollary is detailed in Appendix A.3. Compared to the bound for distributions only with variance available in [13] which is $\mathcal{O}(n\delta^{-1})$, our bound is $\mathcal{O}(n + \ln \delta^{-1})$ and thus less conservative for small δ . We also provide bounds for the moments of the norm of sub-Gaussian random vectors similar to [34, Proposition 2.5.2 (ii)]:

Lemma 3 (Bounds of moments). *Consider $X \sim \mathcal{SG}(\mu, \Sigma)$ with $\mu \in \mathbb{R}^n$ and $\Sigma \succ 0 \in \mathbb{R}^{n \times n}$. For any $p \geq 1$, it holds that*

$$\mathbb{E} [\|X - \mu\|_{\Sigma^{-1}}^p] \leq \underbrace{p 2^{\frac{p-1}{2}} \left(\frac{2e}{n}\right)^{\frac{n}{2}} \Gamma\left(\frac{n+p+1}{2}\right)}_{=: \mathcal{B}(p, n)}$$

where Γ is the Gamma function.

Proof. Similar to [34, Proposition 2.5.2 (ii)], we have:

$$\begin{aligned} \mathbb{E} [\|X - \mu\|_{\Sigma^{-1}}^p] &= \int_0^\infty \Pr\{\|X - \mu\|_{\Sigma^{-1}}^p \geq u\} du \\ &\stackrel{u=t^p}{=} \int_0^\infty \Pr\{\|X - \mu\|_{\Sigma^{-1}} \geq t\} p t^{p-1} dt \\ &\stackrel{\text{Equ. (7)}}{\leq} \left(\frac{e}{n}\right)^{\frac{n}{2}} \int_0^\infty p t^{n+p-1} \exp\left(-\frac{t^2}{2}\right) dt \\ &\stackrel{\tau=\frac{t^2}{2}}{=} p 2^{\frac{p-1}{2}} \left(\frac{2e}{n}\right)^{\frac{n}{2}} \underbrace{\int_0^\infty \tau^{\frac{n+p-1}{2}} e^{-\tau} dt}_{\Gamma\left(\frac{n+p+1}{2}\right)}. \quad \square \end{aligned}$$

Lemma 3 will be useful for analyzing the expected cost in MPC later. Both Lemma 2 and Theorem 2 yield

probabilistic reachable sets that can be leveraged in the stochastic MPC scheme. Lemma 2 is ideal if (2) is a single half-space constraint and it can also be applied for polytope chance constraints. Theorem 2 is capable of handling general constraints.

3.4 Sub-Gaussian stochastic MPC

In this section, we address Problem (5) by extending the stochastic MPC framework [24] from Gaussian to sub-Gaussian noise. As in [24], we consider the propagation of z_t and \hat{x}_t as

$$z_{t+1} = Az_t + Bv_t \quad (10a)$$

$$\hat{x}_{t+1} = A\hat{x}_t + Bu_t + L(y_{t+1} - C(A\hat{x}_t + Bu_t)) \quad (10b)$$

$$u_t = K(\hat{x}_t - z_t) + v_t \quad (10c)$$

where \hat{x}_t is the estimated state, z_t is nominal state with $z_0 = \mu_0$, and v_t is the nominal input. The observer gain L and the feedback K are designed offline, e.g., using linear-quadratic-Gaussian. The error $e_t := [\hat{x}_t - x_t; x_t - z_t] \in \mathbb{R}^{2n_x}$ consisting of estimation error and tracking error satisfies

$$e_{t+1} = A^e e_t + B_1^e w_t + B_2^e \epsilon_t, \quad (11)$$

$$A^e := \begin{bmatrix} A - LCA & 0 \\ -BK & A + BK \end{bmatrix},$$

$$B_1^e := \begin{bmatrix} I - LC \\ I \end{bmatrix}, B_2^e := \begin{bmatrix} -L \\ 0 \end{bmatrix},$$

with A^e Schur-stable by designing K, L properly. By denoting the matrix variance proxy of e_t as Σ_t , we can propagate it through time based on Theorem 1:

$$\Sigma_{t+1} = A^e \Sigma_t A^{e\top} + \sigma_w^2 B_1^e B_1^{e\top} + \sigma_\epsilon^2 B_2^e B_2^{e\top}, \quad (12)$$

where $\Sigma_0 = \sigma_0^2 I$.

To derive PRS, we first define

$$\xi_t := \begin{bmatrix} x_t - z_t \\ u_t - v_t \end{bmatrix} = \begin{bmatrix} 0 & I \\ K & K \end{bmatrix} e_t =: K^e e_t \in \mathbb{R}^{n_x + n_u},$$

Then we have $\xi_t \sim \mathcal{SG}(0, K^e \Sigma_t K^{e\top})$ according to Theorem 1. The set \mathcal{E}_t with $\Pr\{\xi_t \in \mathcal{E}_t\} \geq 1 - \delta$ can be computed as a half-space $\mathcal{E}_t = \mathcal{E}^h(0, K^e \Sigma_t K^{e\top}, \delta, h)$ given a direction h or an ellipsoid $\mathcal{E}_t = \mathcal{E}^e(0, K^e \Sigma_t K^{e\top}, \delta, n_x + n_u)$ as is defined in Lemma 2 and Theorem 2. In case that $\mathcal{X} \times \mathcal{U}$ only has boundaries in a $n_c < n_x + n_u$ -dimensional subspace $\text{span}(H)$ with $H \in \mathbb{R}^{n_c \times (n_x + n_u)}$, we can construct a cylindrical confidence set $\mathcal{E}_t = \mathcal{E}^e(H, \mu, \Sigma, \delta, n_c)$ according to (9). The chance constraints (2) can then be

ensured by the following tightened constraints:

$$(z_t, v_t) \in (\mathcal{X} \times \mathcal{U}) \ominus \mathcal{E}_t.$$

Following [24], the MPC problem at each time step t with horizon H is

$$\min_{v_{0:H-1|t}} \ell_f(\bar{x}_{H|t}) + \sum_{i=0}^{H-1} \ell(\bar{x}_{i|t}, v_{i|t} + K(\bar{x}_{i|t} - z_{i|t})) \quad (13a)$$

$$\text{s.t. } \forall i \in \{0, \dots, H-1\} : \quad (13b)$$

$$z_{i+1|t} = Az_{i|t} + Bv_{i|t}, \quad (13c)$$

$$\bar{x}_{i+1|t} = A\bar{x}_{i|t} + BK(\bar{x}_{i|t} - z_{i|t}) + Bv_{i|t}, \quad (13d)$$

$$(z_{i|t}, v_{i|t}) \in (\mathcal{X} \times \mathcal{U}) \ominus \mathcal{E}_{t+i}, \quad (13e)$$

$$z_{H|t} \in \mathcal{Z}_f, \quad (13f)$$

$$\bar{x}_{0|t} = \hat{x}_t, \quad (13g)$$

$$z_{0|t} = z_t, \quad (13h)$$

where $z_{i|t}, \bar{x}_{i|t}$ denote the nominal and certainty equivalent prediction of the states predicted i steps in the future. The optimal nominal inputs at time step t are denoted by $v_{0:H|t}^*$. Problem (13) minimize the cost of the prediction conditioned on the estimated state, while constraints are enforced through a nominal initialization with the offline computed PRS $\mathcal{E}_{t:t+H-1}$. It is a convex quadratic program if ℓ, ℓ_f are quadratic functions and the constraints are polytopic. We design the terminal set \mathcal{Z}_f and terminal cost ℓ_f such that they satisfy the terminal invariance property:

Assumption 2 (Terminal set and cost [24]). *The terminal set \mathcal{Z}_f and terminal cost ℓ_f satisfy for all $z \in \mathcal{Z}_f$ and all $x \in \mathbb{R}^n$:*

- a. (Positive invariance) $(A + BK)z \in \mathcal{Z}_f$;
- b. (Constraints satisfaction) $(z, Kz) \in (\mathcal{X} \times \mathcal{U}) \ominus \mathcal{E}_t, t \in \mathbb{N}$,
- c. (Lyapunov) $\ell_f((A + BK)x) \leq \ell_f(x) - \ell(x, Kx)$.

Here \mathcal{Z}_f can be designed as the maximal positively invariant set of $\{z \mid (z, Kz) \in (\mathcal{X} \times \mathcal{U}) \ominus \cup_{i=0}^{\infty} \mathcal{E}_i\}$.

The resulting closed-loop system is given by:

$$v_t = v_{0|t}^*, \quad (14)$$

In order to provide closed-loop stability, we also consider the following regularity conditions:

Assumption 3 (Regularity conditions). *The cost is given by $\ell(x, u) = \|x\|_Q^2 + \|u\|_R^2$, $\ell_f(x) = \|x\|_P^2$ with $Q, R, P \succ 0$.*

The matrix P can be computed using the LQR. The closed properties of the controller (14) are summarized in the following theorem:

Theorem 3 (Closed-loop Properties). *Let Assumptions 1 and 2 hold and suppose that Problem (13) is feasible at $t = 0$. Then, the Problem (13) is recursively feasible for all $t \in \mathbb{N}$, and the closed-loop system (1), (14) satisfies the chance constraints (2) for all $t \in \mathbb{N}$. Furthermore, with Assumption 3, the asymptotic average cost satisfies:*

$$\lim_{T \rightarrow \infty} \frac{1}{T} \sum_{t=0}^{T-1} \mathbb{E}[\ell(x_t, u_t)] \leq \kappa_w(\sigma_w) + \kappa_\epsilon(\sigma_\epsilon),$$

where κ_w and κ_ϵ are \mathcal{K}_∞ functions.

The proof is detailed in Appendix A.4. In Theorem 3, the closed-loop constraint satisfaction property provides safety guarantees, while the asymptotic average cost bound implies a low average cost if the variance prox of the noise is small. Compared to [24], Theorem 3 additionally address non-identical noises under sub-Gaussian assumptions.

4 Numerical experiments

In this section, we assess the performance of our uncertainty propagation and MPC methods. For our experiments, we empirically demonstrate that

- (1) The PRS computed by our method satisfies the user-specified containment probability, including heteroscedastic noise settings.
- (2) Our PRS is less conservative than the robust and distributional robust baselines.
- (3) Our MPC approach achieves a smaller cost than robust and DR MPC, while providing probabilistic guarantees on constraint satisfaction in contrast to the Gaussian-based stochastic MPC.

All experiments are conducted with setting the probability threshold to $1 - \delta = 95\%$.

4.1 Environments

We demonstrate the performance of our approach on three different test-beds, as is shown in Figure 2. We first evaluate our choice of sub-Gaussian modeling on two standard examples in the MPC literature, mass-spring-damper and vertical landing. In addition, we consider a problem inspired by robotic spine surgery [35,2]. In this example, noisy state measurements are estimated from high-dimensional inputs. Next, we provide a qualitative description of these examples while additional implementation details can be found in Appendix A.5.

Mass-Spring-Damper (MSD) This classical linear model consists of a mass block, a spring, and a damper. The system input is the force applied to the mass block, while the outputs are the noisy measurements of the

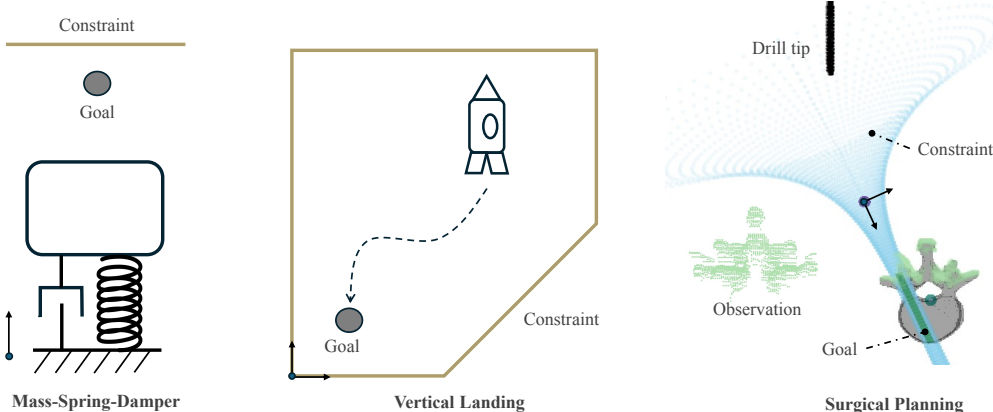


Fig. 2. Illustration of testing control environments: Mass-Spring-Damper, Vertical Landing and Surgical Planning. The constraints are colored yellow and blue respectively. Black arrows represent the coordinate systems.

state. The control problem is to move the object to a target position without going beyond a prespecified position.

Vertical Landing (VL) This system, featured in [32], serves as a simplified model for rocket landing. The state includes 2D position, orientation, and velocities (6 dimensions in total), with inputs consisting of vertical and angular accelerations. The output is the state, measured with noise. We model additional wind fluctuations close to ground by increasing the noise by a factor of 7 for positions below a certain threshold, which results in *heteroscedastic noise*. The task is to land the rocket at a predefined location without violating position constraints. Both vertical and lateral constraints are set close to the target to make the problem more challenging.

Surgical Planning (SP) This environment, taken from [2], provides a simplified model for intraoperative pedicle screw placement, a common step for robotic spine surgery. The state is defined by the relative position between the drill and the goal position, with velocity as the input. This relative pose is estimated through image-based registration between the real-time bone surface reconstruction (green in Figure 2, obtained from simulated ultrasound images) and a given bone mesh model (gray), see Remark 1. Funnel-shaped constraints define a narrow feasible region, ensuring the avoidance of safety-critical structures like nerves and blood vessels, as is shown in Figure 2.

We introduce process noise sampled from various standard distributions for the environments, including Gaussian, Student-t, Laplace, Uniform, and Skew-normal distributions. To ensure the noise remains sub-Gaussian, we apply a maximum bound, truncating the distributions accordingly. The detailed scales and bounds applied in all environments are detailed in Appendix A.5. In MSD and VL environments, process noise distributions are randomly chosen from all these distributions,

whereas SP uses only noise drawn from a Laplace distribution. We also add measurement noise following the same distributions in MSD and VL, while the measurement noise in SP originates from image-based registration used to estimate the relative pose. Since the analytical sub-Gaussian variance proxies are not available for some distributions, we use 5000 samples to calibrate their variance proxies, akin to [4]. Specifically, from Definition 2, it holds that:

$$\sigma^2 = \max_{\lambda \in \mathbb{R}^n} \frac{2 \ln \mathbb{E}[e^{\lambda^\top (X - \mu)}]}{\|\lambda\|^2} \approx \max_{\lambda \in \mathbb{R}^n} \frac{2 \ln \frac{1}{N} \sum_{i=1}^N e^{\lambda^\top (X_i - \hat{\mu})}}{\|\lambda\|^2}$$

where $X_{1:N}$ are data samples and $\hat{\mu}$ is the sample mean.

4.2 Baselines

We consider the following baselines for comparison:

Robust [23,30] The noise terms ϵ_t and w_t are bounded within sets \mathcal{E} and \mathcal{W} respectively, which are calibrated as the maximum bound from samples. The uncertainty propagation in Equation (11) is handled through set propagation: $\mathcal{E}_{t+1} = A\mathcal{E}_t \oplus B_1^e \mathcal{W} \oplus B_2^e \mathcal{E}$, where \oplus is the Minkowski sum.

Stochastic - Gaussian [13,24] In most existing stochastic MPC approaches, the noise is assumed to be zero-mean Gaussian: $\epsilon_t \sim \mathcal{N}(0, \Sigma_\epsilon)$ and $w_t \sim \mathcal{N}(0, \Sigma_w)$. Σ_ϵ and Σ_w are estimated from noise samples as the empirical covariance matrices. Then covariance of errors Σ_t can be computed by linear covariance propagation through the dynamics. The resulting confidence set \mathcal{E}_t can be expressed as $\{e_t \mid e_t^\top \Sigma_t^{-1} e_t \leq \mathcal{C}_{\chi^2_{2n_c}}(1 - \delta)\}$, where $\mathcal{C}_{\chi^2_{2n_c}}$ denotes the quantile function of $\chi^2(2n_c)$ distribution [13].

Distributionally Robust (DR) with Variance-based Ambiguity Sets [13,11] Instead of Gaussian distributions, many works consider formulations

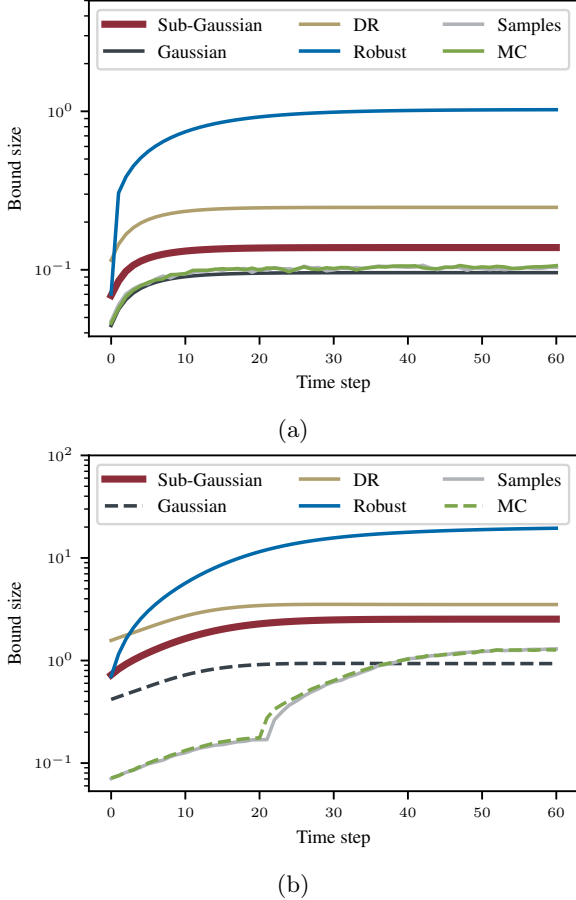


Fig. 3. Comparison of 95% confidence bound sizes quantified by different methods in (a) mass-spring-damper and (b) vertical landing environments. Gray lines represent quantiles from test samples. Approaches with solid curves are valid for the heteroscedasticity of noises by using the global maximum confidence bound, in contrast to those with dashed curves. Specifically, the Gaussian approach assumes an identical distribution of noise. The Monte-Carlo sampling-based (MC) method assumes that the trajectory distributions are identical, but our testing inputs are different from the calibration inputs in VL, resulting in unmatched inlier ratios to the confidence level.

that treat *all distributions* with the given covariance matrix. Specifically, with the same covariance matrix propagated as Stochastic-Gaussian approaches, the bounds are obtained with Chebyshev inequality $\mathcal{E}_t = \{e_t \mid e_t^\top \Sigma_t^{-1} e_t \leq \frac{n_c}{\delta}\}$. In this case, the resulting bounds are distribution-agnostic, which comes at the price of increased conservatism.

Monte-Carlo Sampling (MC) [1,20,7,21] Sampling-based uncertainty quantification has been widely adopted by conformal prediction and scenario approaches. Under the i.i.d. assumption between different trials, we collect N trajectories $\{e_t^j\}_{j=1}^N$ to calibrate the confidence bounds for new trials. We define the score functions as $S_t(e_t) := e_t^\top \Sigma_t^{-1} e_t$, where Σ_t is the

Table 1
Comparison of minimum containment probability over time between different approaches with 95% confidence. Underlined values represent containment probabilities significantly below the predefined threshold (i.e. insufficient coverage).

	MSD	VL	SP
Sub-Gaussian	99.002	98.644	99
Gaussian	<u>89.379</u>	<u>63.589</u>	94
Robust	99.997	100.000	100
DR	99.996	99.999	100
MC	94.781	<u>64.110</u>	94

covariance matrix propagated by Equation (12). We then compute the scores $\{e_t^{j\top} \Sigma_t^{-1} e_t^j\}_{j=1}^N$ and determine their $[(1 - \delta)(N + 1)]/N$ empirical quantile, denoted as $\hat{q}_t(\delta, N)$. The resulting confidence set is given by $\mathcal{E}_t = \{e_t \mid e_t^\top \Sigma_t^{-1} e_t \leq \hat{q}_t(\delta, N)\}$.

4.3 Uncertainty propagation

In this section, we study the performance of our approach compared to the baseline uncertainty propagation methods. To this end, we use different approaches to predict probabilistic reachable sets $\mathcal{E}_{0:T}$ (Section 4.2) conditioned on the same action sequence $u_{0:T}$ under random noises, where T is the total number of steps. We then generate $N = 10^5$ testing trajectories for VL and MSD environments and compute the errors between nominal and true states as $\{e_{0:T}^i\}_{i=1}^N$. For the SP environment, we only generate $N = 100$ testing trajectories due to the complexity of the simulation. In each environment, the MC approach uses the same number of trajectories as testing ones (N) to quantify probabilistic reachable sets. We compare the minimum containment probability $\min_t \Pr\{e_t \in \mathcal{E}_t\}$, which is empirically estimated using N samples. Moreover, we also compare confidence bound sizes ($\sup_{e \in \mathcal{E}_t} a^\top e$) with baselines and quantiles from samples, where a is the normal of the closest constraint boundary of the environment.

The results in Table 1 demonstrate that the confidence bounds from sub-Gaussian propagation satisfy the predefined confidence level. In addition, our approach is also less conservative than the variance-based distributional robust approach, which has a similar containment probability as the robust approach. Figure 3a illustrates that the bound size from our approach is always greater than the quantile bounds from samples and smaller than the robust and DR bounds, highlighting reliability and reduced conservatism of the uncertain prediction. On the contrary, the Gaussian bounds often fail to match the confidence for non-Gaussian noise distributions. The results in Table 1 also show the capability of our approach to provide probabilistic guarantees for heteroscedastic noise in VL. In contrast, the sampling-based approach fails to address the non-identical noise distributions, as

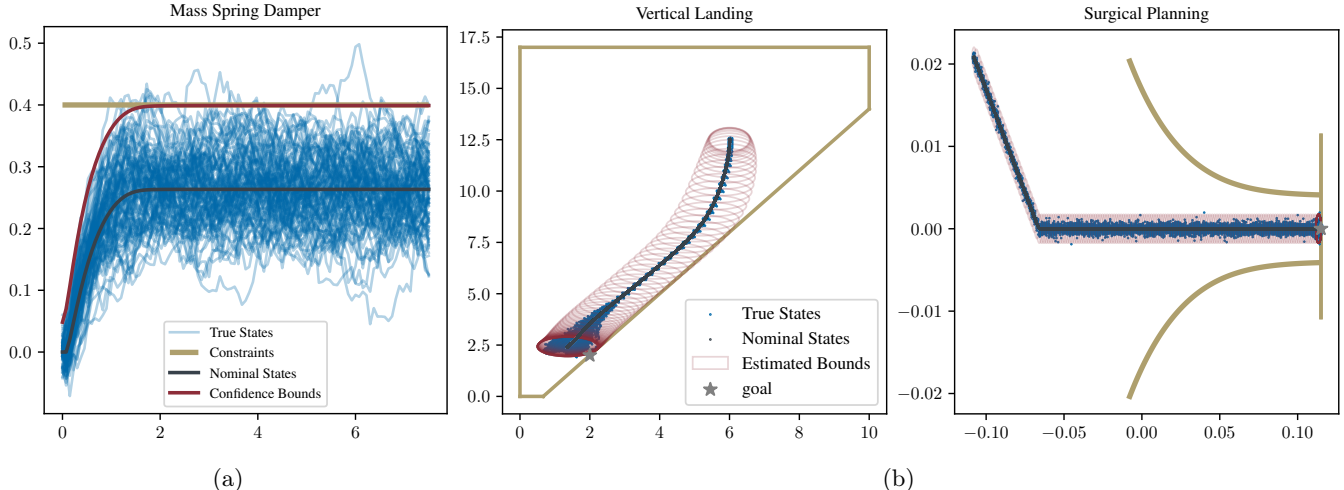


Fig. 4. Plans from our sub-Gaussian MPC approaches in 100 trials from MSD, VL and SP (left to right) environments respectively. For MSD, the x and y axes are time and the first state, respectively. For VL and SP, they correspond to the first 2 dimensions of the states. The confidence levels of displayed examples are set at 95%. The yellow lines represent the boundary constraints. In all problems, the proposed approach satisfies the safety-critical constraints with the chosen probability 95%.

Table 2

Average cost and constraint violation probability for different MPC approaches in different environments. ACP and MCP denote the averaged and maximum constraint violation probability through time, respectively, while the desired maximum value is $\delta = 5\%$. Underlined values represent MCP higher than 5% (violation of chance constraints).

Environments	MSD (Student-t)			VL (Heteroscedastic Gaussian)			SP (Bounded Laplace)			
	Metrics	ACP [%]	MCP [%]	Cost	ACP [%]	MCP [%]	Cost	ACP [%]	MCP [%]	Cost
Sub-Gaussian		1.01	5	3.84	0	0	3014.8	0.01	1	24.985
Gaussian		3.42	<u>10</u>	3.10	0.06	1	2910.5	0.47	4	24.984
DR		0.00	0	6.34	0	0	3877.6	0	0	24.986

is shown in Table 1 and Figure 3b.

4.4 Stochastic MPC

In this section, we evaluate the effectiveness of our approach for output-feedback stochastic MPC. This approach is compared against the same framework under the Gaussian assumption [24] and distributional robust MPC [13]. Robust MPC is not compared with other approaches since it fails to find feasible solutions for all testing environments, which is due to the significantly larger PRS shown in Figure 3. In the MSD environment, we utilize the half-space confidence bounds (Lemma 2) for all stochastic MPC approaches. Elliptical bounds are used for VL and SP environments. The evaluation metrics include the total cost, averaged and maximum constraint violation ratio through time, measured over 100 closed-loop trajectories.

The results in Table 2 show the capability of our approach to satisfy the chance constraints while being less conservative than the distributional robust approaches. In Table 2, our satisfaction of the chance constraints are all greater than 95%, the desired value. Our average costs

are smaller than those of the variance-based distributional robust approach. Finally, Figures 4a and 4b show the confidence sets from our sub-Gaussian approach, which are reasonably small for finding feasible solutions to the considered problems, including SP with vision-based state estimation. Plans and confidence sets from other approaches are detailed in Figures A.1 and A.2.

5 Conclusion

In this work, we proposed a guaranteed stochastic uncertainty propagation framework based on an extended sub-Gaussian definition. We derived sub-Gaussian characterization and confidence bounds for the state distribution resulting from sub-Gaussian noise. We validated our theoretical contributions through sufficient numerical evaluation of our method, demonstrating its capability to guarantee chance constraint satisfaction while being less conservative than robust and distributional robust approaches. Interesting future directions include extending the stochastic MPC to nonlinear systems and leveraging the sub-Gaussian characterization in machine learning.

References

- [1] Anastasios N Angelopoulos and Stephen Bates. A gentle introduction to conformal prediction and distribution-free uncertainty quantification. *arXiv preprint arXiv:2107.07511*, 2021.
- [2] Yunke Ao, Hooman Esfandiari, Fabio Carrillo, Christoph J Laux, Yarden As, Ruixuan Li, Kaat Van Assche, Ayoob Davoodi, Nicola A Cavalcanti, Mazda Farshad, et al. Saferplan: Safe deep reinforcement learning for intraoperative planning of pedicle screw placement. *Medical Image Analysis*, 99:103345, 2025.
- [3] Liviu Aolaritei, Marta Fochesato, John Lygeros, and Florian Dörfler. Wasserstein tube mpc with exact uncertainty propagation. In *2023 62nd IEEE Conference on Decision and Control (CDC)*, pages 2036–2041. IEEE, 2023.
- [4] Julyan Arbel, Olivier Marchal, and Hien D Nguyen. On strict sub-gaussianity, optimal proxy variance and symmetry for bounded random variables. *ESAIM: Probability and Statistics*, 24:39–55, 2020.
- [5] Alberto Bemporad and Manfred Morari. Robust model predictive control: A survey. In *Robustness in identification and control*, pages 207–226. Springer, 2007.
- [6] Stamatis Cambanis, Steel Huang, and Gordon Simons. On the theory of elliptically contoured distributions. *Journal of Multivariate Analysis*, 11(3):368–385, 1981.
- [7] Kong Yao Chee, M. Ani Hsieh, and George J. Pappas. Uncertainty quantification for learning-based mpc using weighted conformal prediction. In *2023 62nd IEEE Conference on Decision and Control (CDC)*, pages 342–349, 2023.
- [8] Glen Chou, Necmiye Ozay, and Dmitry Berenson. Safe output feedback motion planning from images via learned perception modules and contraction theory. In *International Workshop on the Algorithmic Foundations of Robotics*, pages 349–367. Springer, 2022.
- [9] Sayak Ray Chowdhury and Aditya Gopalan. On kernelized multi-armed bandits. In *International Conference on Machine Learning*, pages 844–853. PMLR, 2017.
- [10] Paul Drews, Grady Williams, Brian Goldfain, Evangelos A Theodorou, and James M Rehg. Vision-based high-speed driving with a deep dynamic observer. *IEEE Robotics and Automation Letters*, 4(2):1564–1571, 2019.
- [11] Marcello Farina, Luca Giulioni, Lalo Magni, and Riccardo Scattolini. An approach to output-feedback mpc of stochastic linear discrete-time systems. *Automatica*, 55:140–149, 2015.
- [12] Marcello Farina, Luca Giulioni, and Riccardo Scattolini. Stochastic linear model predictive control with chance constraints—a review. *Journal of Process Control*, 44:53–67, 2016.
- [13] Lukas Hewing, Kim P Wabersich, and Melanie N Zeilinger. Recursively feasible stochastic model predictive control using indirect feedback. *Automatica*, 119:109095, 2020.
- [14] Lukas Hewing and Melanie N Zeilinger. Scenario-based probabilistic reachable sets for recursively feasible stochastic model predictive control. *IEEE Control Systems Letters*, 4(2):450–455, 2019.
- [15] Johannes Köhler and Melanie N Zeilinger. Predictive control for nonlinear stochastic systems: Closed-loop guarantees with unbounded noise. *arXiv preprint arXiv:2407.13257*, 2024.
- [16] Wilbur Langson, Ioannis Chrysochoos, SV Raković, and David Q Mayne. Robust model predictive control using tubes. *Automatica*, 40(1):125–133, 2004.
- [17] Bin Li, Tao Guan, Li Dai, and Guang-Ren Duan. Distributionally robust model predictive control with output feedback. *IEEE Transactions on Automatic Control*, 2023.
- [18] Ruiqi Li, John W Simpson-Porco, and Stephen L Smith. Distributionally robust stochastic data-driven predictive control with optimized feedback gain. *arXiv preprint arXiv:2409.05727*, 2024.
- [19] Zhijun Li, Chenguang Yang, Chun-Yi Su, Jun Deng, and Weidong Zhang. Vision-based model predictive control for steering of a nonholonomic mobile robot. *IEEE Transactions on Control Systems Technology*, 24(2):553–564, 2015.
- [20] Lars Lindemann, Matthew Cleaveland, Gihyun Shim, and George J. Pappas. Safe planning in dynamic environments using conformal prediction. *IEEE Robotics and Automation Letters*, 8(8):5116–5123, 2023.
- [21] Lars Lindemann, Yiqi Zhao, Xinyi Yu, George J Pappas, and Jyotirmoy V Deshmukh. Formal verification and control with conformal prediction. *arXiv preprint arXiv:2409.00536*, 2024.
- [22] Christoph Mark and Steven Liu. Data-driven distributionally robust mpc: An indirect feedback approach. *arXiv preprint arXiv:2109.09558*, 2021.
- [23] David Q Mayne, Saša V Raković, Rolf Findeisen, and Frank Allgöwer. Robust output feedback model predictive control of constrained linear systems. *Automatica*, 42(7):1217–1222, 2006.
- [24] Simon Muntwiler, Kim P Wabersich, Robert Miklos, and Melanie N Zeilinger. Lqg for constrained linear systems: Indirect feedback stochastic mpc with kalman filtering. In *2023 European Control Conference (ECC)*, pages 1–7. IEEE, 2023.
- [25] John P Nolan. Multivariate elliptically contoured stable distributions: theory and estimation. *Computational statistics*, 28:2067–2089, 2013.
- [26] Joel A Paulson, Edward A Buehler, Richard D Braatz, and Ali Mesbah. Stochastic model predictive control with joint chance constraints. *International Journal of Control*, 93(1):126–139, 2020.
- [27] Maria Prandini, Simone Garatti, and John Lygeros. A randomized approach to stochastic model predictive control. In *2012 IEEE 51st IEEE Conference on Decision and Control (CDC)*, pages 7315–7320, 2012.
- [28] S.Joe Qin and Thomas A. Badgwell. A survey of industrial model predictive control technology. *Control Engineering Practice*, 11(7):733–764, 2003.
- [29] J.B. Rawlings, D.Q. Mayne, and M. Diehl. *Model Predictive Control: Theory, Computation, and Design*. Nob Hill Publishing, 2017.
- [30] A. Richards and J. How. Robust model predictive control with imperfect information. In *Proceedings of the 2005, American Control Conference, 2005.*, pages 268–273 vol. 1, 2005.
- [31] Arnab Sarker, Peter Fisher, Joseph E Gaudio, and Anuradha M Annaswamy. Accurate parameter estimation for safety-critical systems with unmodeled dynamics. *Artificial Intelligence*, 316:103857, 2023.
- [32] Jerome Sieber, Alexandre Didier, and Melanie N Zeilinger. Computationally efficient system level tube-mpc for uncertain systems. *arXiv preprint arXiv:2406.12573*, 2024.
- [33] Bruce J Swihart and John P Nolan. Multivariate subgaussian stable distributions in \mathbb{R} . *R Journal*, 14(3), 2022.
- [34] Roman Vershynin. *High-Dimensional Probability: An Introduction with Applications in Data Science*. Number 47

in Cambridge Series in Statistical and Probabilistic Mathematics. Cambridge University Press, 2018.

[35] Charles XB Yan, Benoît Goulet, Julie Pelletier, Sean Jy-Shyang Chen, Donatella Tampieri, and D Louis Collins. Towards accurate, robust and practical ultrasound-ct registration of vertebrae for image-guided spine surgery. *International journal of computer assisted radiology and surgery*, 6:523–537, 2011.

A APPENDIX

A.1 Proof of Lemma 1

Proof. Definition 1 to Definition 2: Let us assume that σ is the variance proxy of X with Definition 1. This means for all $\|b\| = 1$, the scalar random variable $b^\top X$ is σ -sub-Gaussian. Therefore, $\forall \lambda \in \mathbb{R}^n$, $\frac{\lambda^\top (X - \mu)}{\|\lambda\|}$ is σ -sub-Gaussian. Then by Definition 1, we have $\forall \lambda \in \mathbb{R}^n$:

$$\begin{aligned} & \mathbb{E} \left[\exp \left(\lambda^\top (X - \mu) \right) \right] \\ &= \mathbb{E} \left[\exp \left(\|\lambda\| \cdot \frac{\lambda^\top (X - \mu)}{\|\lambda\|} \right) \right] \leq \exp \left(\frac{\|\lambda\|^2 \sigma^2}{2} \right). \end{aligned}$$

Hence, X is sub-Gaussian (Definition 2) with variance proxy $\Sigma = \sigma^2 I$.

Definition 2 to Definition 1: According to Definition 2, there is a variance proxy Σ such that for $\forall \lambda \in \mathbb{R}^n$:

$$\mathbb{E} \left[\exp \left(\lambda^\top (X - \mu) \right) \right] \leq \exp \left(\frac{\|\lambda\|_\Sigma^2}{2} \right)$$

Hence, for any $c \in \mathbb{R}$ and $\lambda \in \mathbb{R}^n$, we have:

$$\begin{aligned} & \mathbb{E} \left[\exp \left(c \lambda^\top X - \lambda^\top \mu \right) \right] = \mathbb{E} \left[\exp \left(c \lambda^\top (X - \mu) \right) \right] \\ & \leq \exp \left(\frac{\|c\lambda\|_\Sigma^2}{2} \right) = \exp \left(\frac{c^2 \|\lambda\|_\Sigma^2}{2} \right). \end{aligned}$$

This means for $\forall \lambda \in \mathbb{R}^n$, $\lambda^\top X$ is sub Gaussian with variance proxy $\|\lambda\|_\Sigma$, which means the random vector X is sub-Gaussian with variance proxy $\sigma^2 = \|\Sigma\|$ by Definition 1. \square

A.2 Proof of Theorem 2

Proof. This proof follows the steps in [9, Lemma 2]. Without loss of generality, suppose $E[X] = \mu = 0$. According to Definition 2, we have for $\forall \lambda \in \mathbb{R}^n$:

$$\mathbb{E} \left[\exp \left(\lambda^\top X - \frac{\|\lambda\|_\Sigma^2}{2} \right) \right] \leq 1.$$

Therefore, for λ sampled from any Gaussian distribution $\lambda \sim \mathcal{N}(0, S^{-1})$, we also have:

$$\int_\lambda \mathbb{E}_X \left[\exp \left(\lambda^\top X - \frac{1}{2} \|\lambda\|_\Sigma^2 \right) \right] p(\lambda) d\lambda \leq 1.$$

Now we compute the left-hand side:

$$\begin{aligned} & \int_\lambda \mathbb{E}_X \left[\exp \left(\lambda^\top X - \frac{1}{2} \|\lambda\|_\Sigma^2 \right) \right] p(\lambda) d\lambda \\ &= \frac{1}{\sqrt{(2\pi)^n \det(S^{-1})}} \mathbb{E}_X \left[\int_\lambda \exp \left(\lambda^\top X - \frac{1}{2} \|\lambda\|_{\Sigma+S}^2 \right) d\lambda \right] \\ &= \frac{1}{\sqrt{(2\pi)^n \det(S^{-1})}} \mathbb{E}_X \left[\exp \left(\frac{1}{2} \|X\|_{(\Sigma+S)^{-1}}^2 \right) \right] \\ & \times \int_\lambda \exp \left(-\frac{1}{2} \|\lambda - (\Sigma + S)^{-1} X\|_{\Sigma+S}^2 \right) d\lambda \\ &= \sqrt{\frac{\det S}{\det(\Sigma + S)}} \mathbb{E} \left[\exp \left(\frac{\|X\|_{(\Sigma+S)^{-1}}^2}{2} \right) \right]. \end{aligned}$$

Therefore for any $S \succ 0$, we have:

$$\mathbb{E} \left[\exp \left(\frac{\|X\|_{(\Sigma+S)^{-1}}^2}{2} \right) \right] \leq \sqrt{\frac{\det(\Sigma + S)}{\det(S)}}.$$

Now let us assign $S = m\Sigma, m > 0$, then we obtain:

$$\mathbb{E} \left[\exp \left(\frac{\|X\|_{\Sigma^{-1}}^2}{2 + 2m} \right) \right] \leq \sqrt{\frac{\det(1 + m)\Sigma}{\det(m\Sigma)}} = \left(\frac{1 + m}{m} \right)^{\frac{n}{2}}.$$

Finally, we get for $\forall m > 0$ and $t \geq 0$:

$$\begin{aligned} & \Pr\{\|X\|_{\Sigma^{-1}} \geq \tau\} \\ &= \Pr \left\{ \exp \left(\frac{\|X\|_{\Sigma^{-1}}^2}{2 + 2m} \right) \geq \exp \left(\frac{\tau^2}{2 + 2m} \right) \right\} \\ & \leq \mathbb{E} \left[\exp \left(\frac{\|X\|_{\Sigma^{-1}}^2}{2 + 2m} \right) \right] \cdot \exp \left(-\frac{\tau^2}{2 + 2m} \right) \quad (\text{A.1}) \\ & \leq \left(\frac{1 + m}{m} \right)^{\frac{n}{2}} \exp \left(-\frac{\tau^2}{2 + 2m} \right), \end{aligned}$$

where the second last inequality is the Chernoff inequality. Now we minimize this tail bound over m :

$$\begin{aligned} & \frac{d}{dm} \left(\frac{1 + m}{m} \right)^{\frac{n}{2}} \exp \left(-\frac{\tau^2}{2(1 + m)} \right) = 0 \\ & \Rightarrow \left(-\frac{n}{2m^2} + \frac{\tau^2}{2(1 + m)m} \right) = 0 \Rightarrow m^* = \frac{n}{\tau^2 - n}, \end{aligned}$$

where $\tau^2 - n > 0$ by assumption. Plugging m^* to Inequality (A.1) yields:

$$\Pr\{\|X\|_{\Sigma^{-1}} \geq \tau\} \leq \left(\frac{\tau^2}{n}\right)^{\frac{n}{2}} \exp\left(\frac{n - \tau^2}{2}\right),$$

which can be rearranged as Equation (7). Abbreviating $s := \frac{\tau^2}{n} - 1$ and assigning the tail probability to δ , we have:

$$\left(\frac{\exp(s)}{1+s}\right)^{\frac{n}{2}} = \frac{1}{\delta} \Rightarrow \frac{\exp(s)}{1+s} = \delta^{-\frac{2}{n}}. \quad (\text{A.2})$$

Therefore, $s = g^{-1}\left(\delta^{-\frac{2}{n}}\right)$ and the confidence bound is solved as $\tau^2 = n + ng^{-1}\left(\delta^{-\frac{2}{n}}\right)$ as in Equation (8). \square

A.3 Proof of Corollary 1

Proof. Denote $s = g^{-1}(\delta^{-\frac{2}{n}})$ and $\tau^2 = n(s+1)$. Since $1+s \leq 2\exp(\frac{s}{2}) - 1$ for $s \geq 0$, we have:

$$\begin{aligned} \frac{\exp(s)}{2\exp(\frac{s}{2}) - 1} &\leq \frac{\exp(s)}{1+s} = \delta^{-\frac{2}{n}} \\ \Leftrightarrow \exp(s) - 2\delta^{-\frac{2}{n}} \exp\left(\frac{s}{2}\right) + \delta^{-\frac{2}{n}} &\leq 0. \end{aligned}$$

Since the left-hand side is a quadratic function of $\exp(\frac{s}{2})$, it holds:

$$\begin{aligned} \exp\left(\frac{s}{2}\right) &\leq \delta^{-\frac{2}{n}} + \sqrt{\delta^{-\frac{4}{n}} - \delta^{-\frac{2}{n}}} \\ \Rightarrow \tau^2 &\leq n + 2n \ln\left(\delta^{-\frac{2}{n}} + \sqrt{\delta^{-\frac{4}{n}} - \delta^{-\frac{2}{n}}}\right) \\ &\leq n + 2n \ln\left(2\delta^{-\frac{2}{n}}\right) \\ &= (1 + 2\ln 2)n + 4 \ln \delta^{-1}. \quad \square \end{aligned}$$

A.4 Proof of Theorem 3

Proof. The proof follows the arguments of [15, Thm. 2] and [24, Thm. 1].

Recursive feasibility: Given the optimal input $v_{0:H-1|t}^*$ at some time t , we assign $v_{H|t}^* := Kz_{H|t}^*$. For time $t+1$, we consider the candidate inputs $v_{0:H-1|t+1} = v_{1:H|t}^*$, which yields the nominal states $z_{0:H|t+1} = \{z_{1:H|t}^*, (A+BK)z_{H|t}^*\}$ using Equations (13c) and (14). This is a feasible candidate solution to Problem (13) using Assumption 2, $(z_{i|t+1}, v_{i|t+1}) = (z_{i+1|t}^*, v_{i+1|t}^*) \in (\mathcal{X} \times \mathcal{U}) \ominus \mathcal{E}_{i+t+1}$, $i \in \{0, 1, \dots, H-1\}$, and $z_{H|t+1} = (A+BK)z_{H|t} \in \mathcal{Z}_f$.

Chance constraints: Even though the error ξ_t is not

necessarily independent of the MPC input v_t , Theorem 1 ensures that $\xi_t \sim \mathcal{SG}(0, \Sigma_t^\xi)$ and the design of \mathcal{E}_t (Thm. 2/Lemma 2) ensures $\Pr\{\xi_t \in \mathcal{E}_t\} \geq 1 - \delta$, $\forall t \in \mathbb{N}$. Thus, closed-loop constraints satisfaction follows with $(x_t, u_t) = (z_t, v_t) + \xi_t \in (z_t, v_t) \oplus \mathcal{E}_t \subseteq \mathcal{X} \times \mathcal{U}$ from the constraint (13e).

Performance guarantees: We denote $u_{i|t}^* = v_{i|t}^* + K(\bar{x}_{i|t}^* - z_{i|t}^*)$, $i = 0, \dots, H$, which satisfies $u_{H|t}^* = K\bar{x}_{H|t}^*$. The optimal certainty equivalent states $\bar{x}_{0:H+1|t}^*$ are determined by (13g) and $\bar{x}_{i+1|t}^* = A\bar{x}_{i|t}^* + Bu_{i|t}^*$, $i = 0, \dots, H$. From Equation (10b), (13g) and (1), we have:

$$\begin{aligned} \bar{x}_{0|t+1} &= \hat{x}_{t+1} = \bar{x}_{1|t}^* + L(y_{t+1} - C\bar{x}_{1|t}^*) \\ &= \bar{x}_{1|t}^* + L(C(Ax_t + Bu_t + w_t) + \epsilon_t - CA\hat{x}_t - CBu_t) \\ &= \bar{x}_{1|t}^* + LCA\hat{e}_t + LCw_t + L\epsilon_t =: \bar{x}_{1|t}^* + \bar{e}_t. \quad (\text{A.3}) \end{aligned}$$

Using $x_t = \hat{x}_t + \hat{e}_t$, the quadratic stage cost satisfies

$$\frac{1}{2}\ell(x_t, u_t) \leq \ell(\hat{x}_t, u_t) + \|\hat{e}_t\|_Q^2. \quad (\text{A.4})$$

We denote $\mathcal{J}_H(t)$ as the optimal objective function of Problem (13) at time t . Following the arguments in [15, Thm 2, proof (i)] and Equation (A.3), the quadratic cost and Lipschitz continuous dynamics ensure

$$\frac{1}{1+m}\mathcal{J}_H(t+1) \leq \mathcal{J}_H(t) - \ell(\hat{x}_t, u_t) + \frac{c_{\mathcal{J}}}{m}\|\bar{e}_t\|^2 \quad (\text{A.5})$$

for all $m > 0$ with a uniform constant $c_{\mathcal{J}} > 0$. We now consider the upper bound for $\text{tr}(\Sigma_\infty)$. The variance propagation (12) and A^e Schur stable imply that:

$$\text{tr}(\Sigma_\infty) \leq c_1(\sigma_\epsilon^2 + \sigma_w^2) \quad (\text{A.6})$$

for some constant $c_1 > 0$. Furthermore, Theorem 1 and (A.3) ensure $\bar{e}_t \sim \mathcal{SG}(0, \bar{\Sigma}_t)$, $\hat{e}_t \sim \mathcal{SG}(0, \hat{\Sigma}_t)$ with

$$\begin{aligned} \hat{\Sigma}_\infty &= [I; 0]\Sigma_\infty[I; 0]^\top, \\ \bar{\Sigma}_\infty &= L(C(A\hat{\Sigma}_\infty A^\top + \sigma_w^2 I)C^\top + \sigma_\epsilon^2 I)L^\top. \end{aligned}$$

This further implies:

$$\begin{aligned} \text{tr}(\hat{\Sigma}_\infty) &\leq \text{tr}(\Sigma_\infty) \\ \text{tr}(\bar{\Sigma}_\infty) &\leq c_2(\text{tr}(\Sigma_\infty) + \sigma_\epsilon^2 + \sigma_w^2) \quad (\text{A.7}) \end{aligned}$$

for some constant $c_2 > 0$. Applying Lemma 3 with $p = 2$ in combination with (A.6) and (A.7) implies:

$$\begin{aligned} \mathbb{E}[\|\bar{e}_t\|^2] &\leq \text{tr}(\bar{\Sigma}_t)\mathbb{E}[\|\bar{e}_t\|_{\bar{\Sigma}_t^{-1}}^2] \leq \mathcal{B}(2, n_x)\text{tr}(\bar{\Sigma}_t) \\ \mathbb{E}[\|\hat{e}_t\|_Q^2] &\leq \mathcal{B}(2, n_x)\lambda_{\max}(Q)\text{tr}(\hat{\Sigma}_t), \quad (\text{A.8}) \end{aligned}$$

where we use $\lambda_{\max}(\Sigma) \leq \text{tr}(\Sigma)$. Combining (A.4), (A.5) and (A.8) yields

$$\begin{aligned} & \mathbb{E}_{\epsilon_t, w_t} \left[\frac{1}{1+m} J_H(t+1) - J_H(t) + \frac{1}{2} \ell(x_t, u_t) \right] \\ & \leq \mathcal{B}(2, n_x) \left(\lambda_{\max}(Q) \text{tr}(\hat{\Sigma}_t) + \frac{c_J}{m} \text{tr}(\bar{\Sigma}_t) \right). \end{aligned}$$

Finally, following [15, (iii), proof Thm. 2], we choose $m > 0$ sufficiently small to arrive at

$$\begin{aligned} & \lim_{T \rightarrow \infty} \mathbb{E}_{\epsilon_{0:T}, w_{0:T}} \left[\frac{1}{T} \sum_{t=0}^{T-1} \ell(x_t, u_t) \right] \\ & \leq \lim_{T \rightarrow \infty} \frac{1}{T} \sum_{t=0}^{T-1} \left(\kappa_1 (\text{tr}(\bar{\Sigma}_t)) + \kappa_2 (\text{tr}(\hat{\Sigma}_t)) \right) \\ & = \kappa_1 (\text{tr}(\bar{\Sigma}_\infty)) + \kappa_2 (\text{tr}(\hat{\Sigma}_\infty)) \\ & \stackrel{(A.7), (A.6)}{\leq} \kappa_w (\sigma_w) + \kappa_\epsilon (\sigma_\epsilon). \quad \square \end{aligned}$$

A.5 Environment Details

In this section, we present the implementation details of our testing environments. The parameters for the noise distributions are shown in Table A.1. In the following, we detail the dynamics, objective function, and constraints of each environment.

A.5.1 Mass-Spring-Damper (MSD)

A 1D MSD system has the form $m\ddot{s} + b\dot{s} + ks = f$, where s is the position, m is the mass, b is the damping coefficient and k is the spring constant. By defining $x = [s, \dot{s}]^\top$, $u = f$, and discretize the system with time Δt , one can obtain the linear system equation of the form:

$$x_{t+1} = \begin{bmatrix} 1 & \Delta t \\ -\frac{k\Delta t}{m} & 1 - \frac{b\Delta t}{m} \end{bmatrix} x_t + \begin{bmatrix} 0 \\ \frac{\Delta t}{m} \end{bmatrix} u_t + w_t$$

We choose $\Delta t = 0.1$, $m = 2$, $k = 1$ and $b = 1$. The observation model is simply $y_t = x_t + \epsilon_t$. Here w_t and ϵ_t can be sampled from any distributions in Section 4.1.

The target state is defined as $x^* = [0.5, 0.0]^\top$, and our total cost is defined as $\sum_{t=1}^T \|x_t - x^*\|^2$, where T is the maximum time step. The constraint is defined as $x_t[0] \leq 0.5, \forall 0 \leq t \leq T$, where $[\cdot]$ denotes the index of dimension. The goal can be translated as getting as close as possible to the target state without exceeding it.

A.5.2 Vertical Landing

The details of this environment are explained in [32]. Here we substitute the uncertainty of modeling with the

additive process noise. The resulting A , B and C matrices of the linear system are:

$$\begin{aligned} A &= \begin{bmatrix} 1.0 & 0.0 & 0.0 & 0.075 & 0.0 & 0.0 \\ 0.0 & 1.0 & 0.0 & 0.0 & 0.075 & 0.0 \\ 0.0 & 0.0 & 1.0 & 0.0 & 0.0 & 0.075 \\ 0.0 & 0.0 & 0.3 & 1.0 & 0.0 & 0.0 \\ 0.0 & 0.0 & 0.0 & 0.0 & 1.0 & 0.0 \\ 0.0 & 0.0 & 0.375 & 0.0 & 0.0 & 1.0 \end{bmatrix} \\ B &= \begin{bmatrix} 0.0 & 0.0 \\ 0.0 & 0.0 \\ 0.0 & 0.0 \\ 0.0 & 0.0 \\ 0.075 & 0.0 \\ 0.0 & 0.5208 \end{bmatrix} \quad C = I_{6 \times 6} \end{aligned}$$

Heteroscedastic noises are introduced by modifying the scale parameter in Table A.1 as

$$s = \begin{cases} 5 \times 10^{-3}, & x[1] > 4.5 \\ 3.5 \times 10^{-2}, & x[1] < 4.5 \end{cases}$$

The goal state is $x^* = [2.0, 2.0, 0.0, 0.0, 0.0, 0.0]^\top$. The trajectory cost function is defined as $\sum_{t=1}^T \|x_t - x^*\|^2 + 0.1 \|u_t\|^2$. The modified polytopic constraints for all $0 \leq t \leq T$ are:

$$\begin{aligned} 0 & \leq x_t[0] \leq 10 \\ 0 & \leq x_t[1] \leq 17 \\ x_t[1] & \geq x_t[0] - 0.7 \end{aligned}$$

which also constructs a narrow feasible region close to the goal state for more effective comparison between different approaches.

A.5.3 Surgical Planning

The original surgical planning system outputs a point cloud observation I_t at each time step (possibly from ultrasound imaging), which is used to estimate the position of the vertebra (p_t). Specifically, given a bone model M from a preoperative image, one can register the bone model to I_t by maximizing the overlap:

$$\tilde{p}_t = \arg \max_p |I_t \cap (M \oplus p)|,$$

where $M \oplus p$ means adding each point of M with p . $|\cdot|$ means the volume of intersection between voxelized

Table A.1

Parameters of noise distributions in our environments. PDF abbreviates probability density function. All dimensions of noise are mutually independent and share the same PDF shown in the table. We use b to denote the maximum norm bound to truncate the distribution.

Distributions	PDF	MSD	VL	SP
Gaussian	$\frac{1}{\sqrt{2\pi}\sigma} \exp\left(-\frac{X^2}{2\sigma^2}\right)$	$\sigma = 0.015$	$\sigma = 0.005$	-
Student-T	$\frac{\Gamma(\frac{v+1}{2})}{s\sqrt{\pi v}\Gamma(\frac{v}{2})} \left(1 + \frac{x^2}{s^2 v}\right)^{-\frac{v+1}{2}}$	$s = 0.015, v = 5, b = 5.0$	$s = 0.005, v = 5, b = 10.0$	-
Laplace	$\frac{1}{2s} \exp\left(-\frac{ x }{s}\right)$	$s = 0.015, b = 5.0$	$s = 0.005, b = 10.0$	$s = 0.2, b = 2.0$
Uniform	$\frac{1}{2b}, X \in [-b, b]$	$b = 0.015$	$b = 0.005$	-
Skew-norm	$\frac{2}{2\pi s} e^{-\frac{(x+\xi)^2}{2s^2}} \int_{-\infty}^{\alpha\frac{x+\xi}{s}} e^{-\frac{t^2}{2}} dt,$ $\xi = s\sqrt{\frac{2\alpha^2}{\pi(1+\alpha^2)}}$	$\alpha = 0.005, s = 0.005$	$\alpha = 0.005, s = 0.005$	-

point clouds. To allow efficient computation, we perform zeroth-order optimization by selecting the optimum from N random particles $p_t^{1:N}$ within a bounded set S_p :

$$\tilde{p}_t = \arg \max_{p_t^1, \dots, p_t^N} |I_t \cap (M \oplus p_t^i)|, \quad p_t^{1:N} \sim \text{Uniform}(S_p)$$

Given the drill pose $[p_t^d, q_t^d]^\top$ (with position p_t^d and sphere coordinate angles $q_t^d \in \mathbb{R}^2$), the resulting per-step estimated state is $\tilde{x}_t = [p_t^d - \tilde{p}_t, q_t^d]^\top$. By assigning $y_t := \tilde{x}_t$, the transformed dynamics is simply 2D 1st order integrator:

$$\begin{aligned} x_{t+1} &= x_t + u_t \Delta t + w_t \\ y_t &= x_t + \epsilon_t \end{aligned}$$

where $\Delta t = 0.075$, ϵ_t is the per-step state estimation error. The goal state is $x^* = [0.12, 0.0]^\top$. The trajectory cost function is defined as $\sum_{t=1}^T \|x_t - x^*\|^2 + 0.001 \|u_t\|^2$. The safety constraint sets for all $0 \leq t \leq T$ are described by:

$$\begin{aligned} \|x_t[1:2]\| &\leq \frac{1}{5} \underbrace{\sqrt{\exp(-2500x_t[0]^2 - 5) + 0.0004}}_{=:g(x_t[0])}, \\ x[0] &\leq 0.12 \end{aligned} \quad (\text{A.9})$$

where a funnel-like narrow feasible region is constructed as illustrated in Figure 4b.

We now compute the constraint tightening for satisfaction probability $1 - \delta$. We construct an ellipsoid \mathcal{E}_t in 3-dimensions by applying Theorem 2 and (9) with $H = [I_{3 \times 3}, 0_{3 \times (n-3)}]$. Then we obtain its longest radius in YZ plane as r_t^{yz} and its length along x axis as r_t^x . Next, we derive the tightened constraints for the non-linear constraint (A.9). First, note that the function g is Lipschitz continuous with constant 0.5. Thus, for any $z \in \mathbb{R}^n$ and $x \in \mathcal{E}_t \oplus \{z\}$, it holds that

$$\|x[1:2]\| - g(x[0]) \leq \|z[1:2]\| + r_t^{yz} - g(z[0]) + 0.5r_t^x.$$

Thus, the following constraint tightening ensure satisfaction of the chance constraints:

$$\|z_t[1:2]\| - g(z_t[0]) + 0.5r_t^x + r_t^{yz} \leq 0, \quad z[0] \leq 0.12 - r_t^x.$$

A.6 Illustration of PRS and Planning Trajectories of Different MPC Approaches

The trajectories and PRS of different approaches in MSD, VL and SP environments are illustrated in Figures A.1 and A.2. In general, DR SMPC generates more conservative trajectories that are further from the constraints. On the contrary, more violations of constraints can be observed for the Gaussian SMPC approach, because Gaussian assumptions cannot capture non-Gaussian noises.

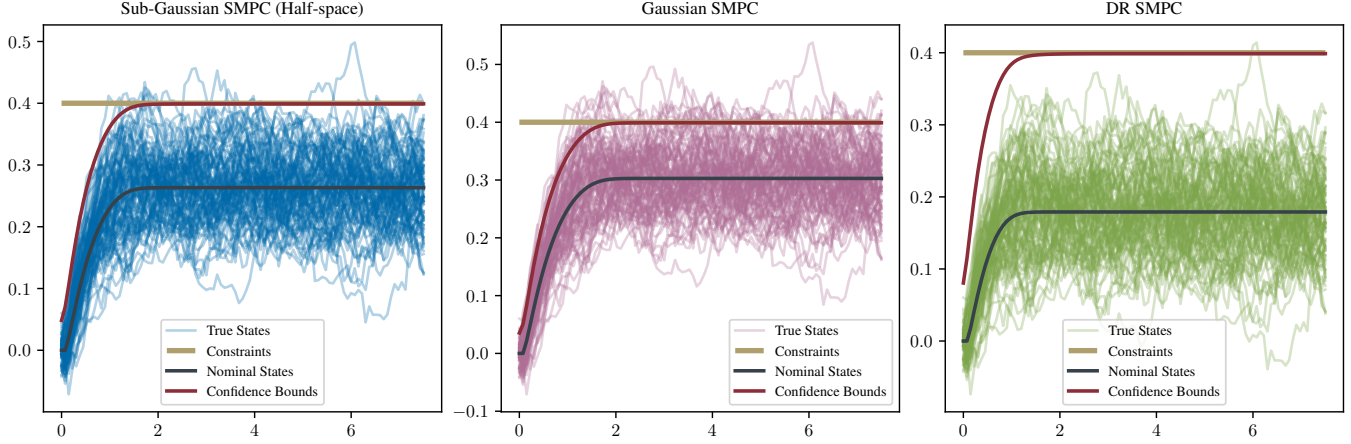


Fig. A.1. Trajectories from different approaches in 100 trials from the MSD environment. The confidence levels of displayed examples are set at 95%. The solid red lines illustrate the boundary of confidence sets. The solid yellow lines represent the boundary constraints. In all problems, the proposed approach satisfies the safety-critical constraints with the chosen probability 95%. DR SMPC generates more conservative trajectories that are further from the constraints.

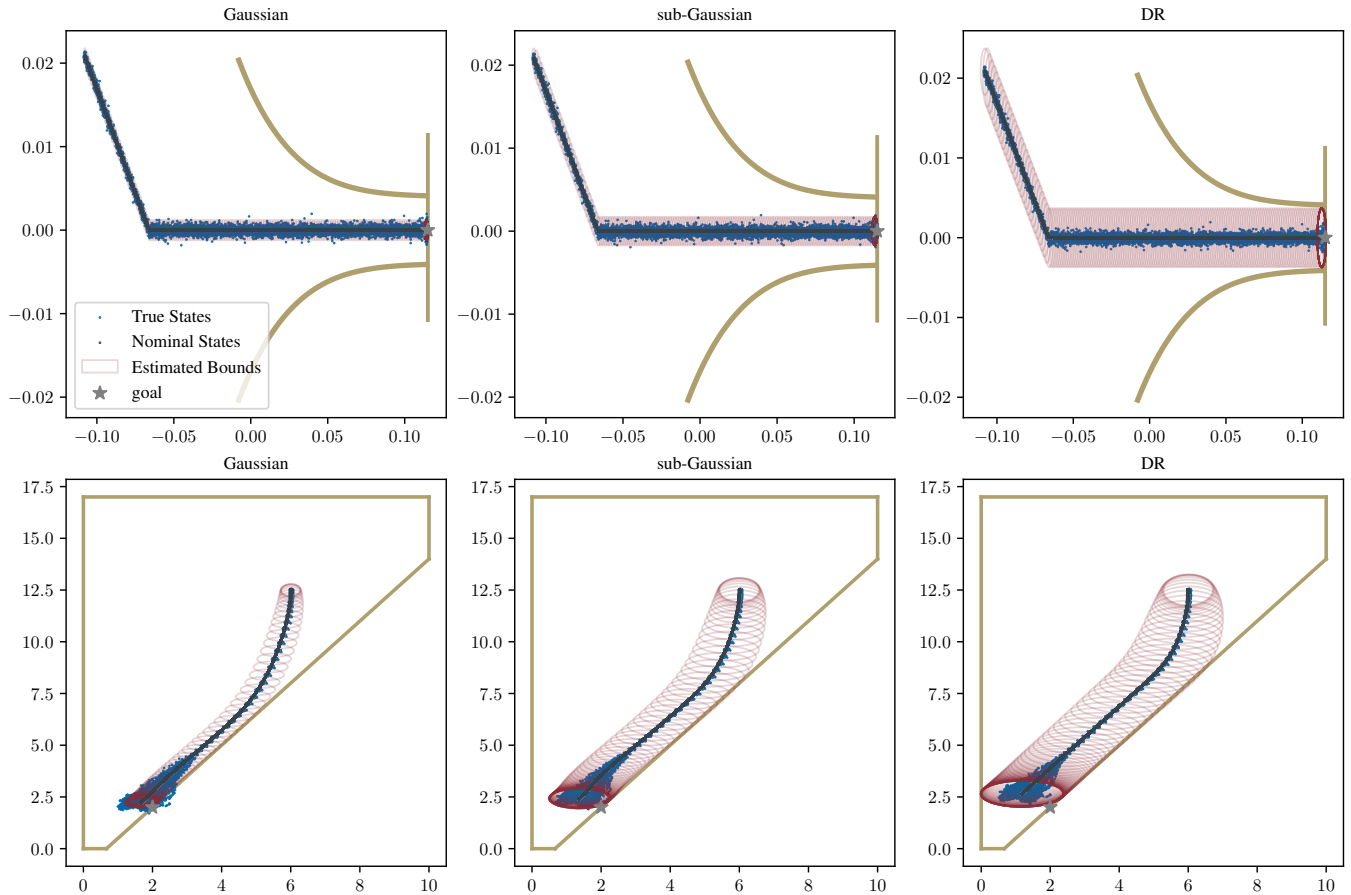


Fig. A.2. Trajectories from different MPC approaches in 100 trials from the SP and VL environments. The confidence levels of displayed examples are set at 95%. Red ellipsoids illustrate probabilistic reachable sets (PRS) from different approaches. The yellow solid lines represent the boundary constraints. In all problems, the proposed approach satisfies the safety-critical constraints with the chosen probability 95%. The PRS of DR SMPC are larger than those of sub-Gaussian and Gaussian approaches, resulting in more conservative trajectories that are further from the constraints.